Early-stage growth of GeTe on Si(111)-Sb

Boris Croes, Fabien Cheynis, Yannick Fagot-Revurat, Pierre Müller, Stefano Curiotto, Frédéric Leroy

Early-stage growth of GeTe on Si(111)-Sb

B. Croes,[1] F. Cheynis,[1] Y. Fagot-Revurat,[2] P. Müller,[1] S. Curiotto,[1] and F. Leroy[1]

[1] *Aix Marseille Univ, CNRS, CINAM, AMUTECH, Marseille, France*

[2] *Univ Lorraine, CNRS, IJL, F-54000 Nancy, France*

(Dated: December 16, 2022)

The advent of germanium telluride as a promising ferroelectric Rashba semiconductor for spintronic applications requires the growth of nanometer-thick films of high crystalline quality. In this study, we have elucidated the initial growth stages of GeTe on Si(111)-Sb by scanning tunneling microscopy and low energy electron diffraction. We demonstrate the presence of an initial 0.35 nm-thick GeTe buffer layer followed by the 2D growth of GeTe *via* Frank-Read sources of atomic steps. As shown by core level spectroscopy, Sb is acting as a surfactant during growth up to a 5 nm-thick film. X-ray diffraction, transmission electron microscopy and low energy electron microscopy evidence that numerous mirror domains and in-plane misorientations appear early in the growth process and are gradually buried at the film/substrate interface. The use of a miscut Si substrate close to Si(111) allows suppressing these defects since the early beginning of growth.

Among ferroelectrics, a new class of materials with high potentialities for spintronic applications has been introduced and known as ferroelectric Rashba semiconductors [1]. In this context α-GeTe exhibits spin-polarized electronic states with the largest Rashba parameter currently reported. Considerable effort has been devoted to the experimental characterization of its electronic band structure [2–5]. Major results have been obtained on α-GeTe thin films. It has been demonstrated the reversal of the ferroelectric polarization under an electric field [6] and a consistent change of the spin chirality of the band structure [7 and 8]. Even more fascinating GeTe thin films have shown remarkable transport properties at RT such as non-reciprocal charge transport [9] or ferroelectric switching of the spin-to-charge conversion [10]. All these results take advantage of the ferroelectric property of the α-GeTe phase. This phase has a rhombohedral structure (space group R3m) and bulk Curie temperature well above RT ($T_c \sim 650-700$ K). The spontaneous polarization of α-GeTe is along the pseudocubic $< 111 >$ leading to the formation of 4 ferroelastic variants. Different substrates have been used to grow GeTe thin films, Si(001) [11 and 12], Si(111) [30], Si(111)-H [14], Si(111)-Sb [15], BaF_2(111) [16 and 17] or InP(111) [8]. As reported by Wang et al. [15] α-GeTe thin films with a quasi-single crystalline quality can be grown on Si(111) by molecular beam epitaxy using a pre-deposition of 1 monolayer of Sb onto the substrate. Despite a significant lattice mismatch of $\sim$8.5% with the reconstructed substrate, the GeTe layer is relaxed since the very beginning of growth. Croes et al. [18] have shown that GeTe thin films thinner than 30 nm have a unique polarization state perpendicular to the film surface. This single polarization state provides the opportunity to address the persistence of ferroelectricity in nanometer-thick films and its fundamental relationship with the spin texture and transport properties. However the growth process of GeTe thin films has been overlooked in the low thickness regime. *In situ* reflection high energy electron diffraction (RHEED) measurements have shown that GeTe thin films are crystalline since the beginning of growth [19]. It has also been shown, by Raman spectroscopy, that the rhombohedral distortion of α-GeTe occurs at $\sim$ 0.7 nm of deposition through the Peierls distortion [19]. Complementary measurements by atomic force microscopy have suggested that the surface of a 2 nm-thick GeTe film exhibits a smooth two-dimensional morphology [15]. However the growth mechanisms in the nanometer-thick film regime are still unknown as well as the nature and density of defects. Their understanding and control are crucial in the context of GeTe thin film optimization with respect to future spintronic-based applications.

In this article we address the structure and morphology of GeTe thin films during the very first stages of growth on Si(111)-Sb. Using scanning tunneling microscopy (STM) we show that GeTe thin films grow initially *via* a homogeneous and crystalline buffer layer. Then atomically flat 2D islands of GeTe nucleate and grow preferentially at Si step edges with a typical size of 50 nm at T=275°C. For a 0.7 nm-thick film, an interfacial relaxation mechanism occurs *via* threading dislocations (Frank-Read sources) that promotes a layer-by-layer growth mode. This process is rapidly dominated by a step-flow growth mode of GeTe layers. Despite a high quality of the surface morphology, a significant amount of mirror domains and in-plane misorientations between adjacent grains is evidenced by low energy electron diffraction (LEED) and dark-field low energy electron microscopy (LEEM). These defects are buried close to the interface with the Si substrate and strongly decay with the film thickness. An alternate growth method using a miscut silicon substrate successfully suppresses these defects.

I. EXPERIMENTAL SECTION

Si(111) wafers (Siltronix; 550 μm -thick; ρ=1-10 Ωcm) are first cleaned by acetone and ethanol rinsing before introduction in ultra-high vacuum (UHV, 10^{-8} Pa). Then the substrates are degassed at 1000 K during 12 h followed by repeated high temperature annealing (1500 K)

during a few minutes in order to obtain a clean 7×7 surface reconstruction. The substrate surface and subsequent growth are characterized by *in situ* RHEED (figure 1). First a deposition of 1 monolayer of Sb is performed on the Si(111) surface, forming the so-called Si(111)-$\sqrt{3}\times\sqrt{3}$-Sb reconstruction that greatly improves the crystalline quality of the GeTe film [15]. The GeTe thin films are grown by co-deposition of Ge (1175 °C) and Te (310 °C) in UHV on a sample maintained at 275°C. In these conditions the flux ratio between Ge:Te is fixed at 2:5 in order to compensate the high desorption rate of Te [12]. All the deposition sources are effusion cells from MBE-Komponenten Gmbh. After growth, the samples are transferred under UHV conditions thanks to a homemade transfer suitcase and characterized by scanning tunneling microscopy (STM) with a VT-STM (Scienta Omicron Gmbh), by LEEM and LEED using a LEEM III microscope (Elmitec GmbH). STM images were obtained at room temperature in constant current mode with typical imaging conditions (U=-1 V, I= 20 pA, W tip). LEED patterns were measured at 16 eV and 26 eV incident electron energies. To quantify the presence of mirror domains, LEED and dark-field LEEM images of the GeTe surface are performed at 26 eV incident electron energy where a high contrast is achieved. The internal structure of thick GeTe films (>40 nm) has been studied by X-ray diffraction at BM32 beamline (ESRF) and TEM. X-ray diffraction data have been measured at 18 keV [λ=0.06888 nm] with a beam size of 200 × 300 μm^2 and collected onto a 2D detector. The data have been converted from the detector coordinates (pixel index) to diffraction angles and then to reciprocal space coordinates. The 3D reciprocal space maps have been visualized using the ParaView software. TEM investigations were performed using [1$\bar{1}$0] zone axis at an accelerating voltage of 300 kV on a JEOL JEM-3010 instrument with a spatial resolution of 0.17 nm. Using focused ion beam preparation procedure (Dual beam FIB, FEI Helios 600 NanoLab), electron transparent ultra-thin sections were extracted from the thin films of GeTe on Si. The typical dimensions of the electron transparent ultrathin sections are 15 μm (length) × 5 μm (height) × 150–200 nm (thickness). Considering surface chemical composition, core level photoemission peaks were measured at CASSIOPEE beamline (Synchrotron SOLEIL, France) using a 800 eV incident photon energy. A typical energy resolution of around 100 meV is achieved, using a Scienta R4000 electron-analyzer with a 0.5 mm entrance slit and a pass-energy of 100 eV. To protect the GeTe surface from contamination during sample transfer to SOLEIL synchrotron UHV chamber, a Te capping was used. The capping is removed in UHV first by a mild Ar ion bombardment at RT (1 keV, 10 μA) to remove the top most oxidized layers then by annealing at 220 °C to desorb the complete Te layer (see supplementary material S1 [20]). Apart from structural, morphological and chemical aspects the GeTe thick film quality has also been checked with respect to electric conductivity (see supplementary material S2 [21])

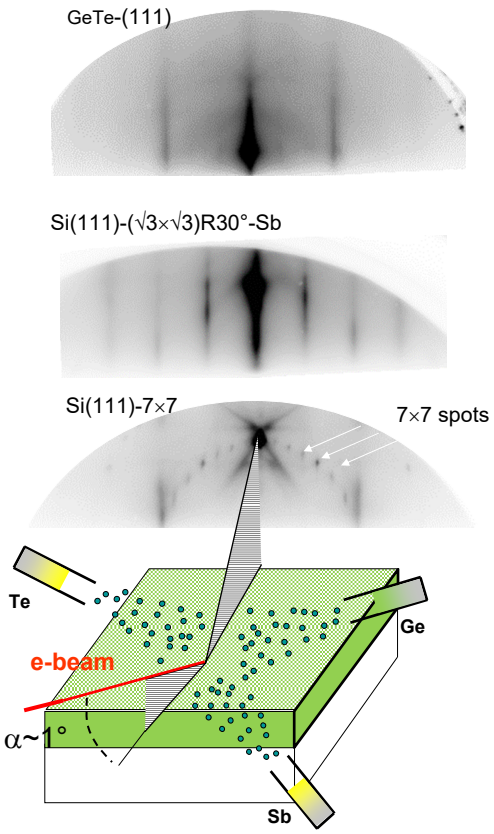

FIG. 1. Experimental protocol of GeTe growth. RHEED patterns of Si(111)-7×7 surface (bottom), Si(111)-$\sqrt{3}\times\sqrt{3}$-Sb reconstruction (middle) and GeTe thin film of 3 nm thickness (top).

II. RESULTS AND DISCUSSION

A. Initial growth of GeTe thin film

The surface morphology of a 0.35 nm-thick GeTe film (1 bilayer of bulk α-GeTe) grown on Si(111)-$\sqrt{3}\times\sqrt{3}$-Sb surface shows a homogeneous grainy aspect [figure 2(a)]. This layer will be called the buffer layer. The measured step height on the surface is 0.31 nm and corresponds to the atomic step height of the Si(111) surface [figure 2(b)]. Despite the granular aspect of the GeTe layer a crystalline order occurs as shown by LEED [figure 2(c)]. The main diffraction peaks of GeTe are perfectly aligned with Si diffraction peaks. This indicates a preferential epitaxy such that GeTe(111)||Si(111) and GeTe[1$\bar{1}$0]||Si[1$\bar{1}$0] in pseudocubic coordinates [15]. The measured in-plane lattice parameter mismatch between Si and GeTe is 8.3%±2.5% [figure 2(e)]. Therefore the in-plane lattice parameter of GeTe is 0.416±0.010 nm considering that the interatomic distance between Si atoms is

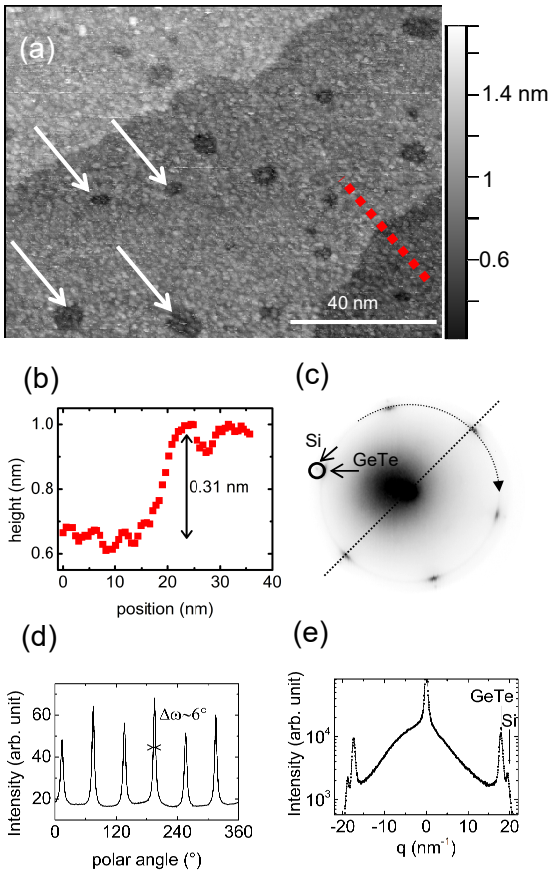

FIG. 2. (a) STM image of a 0.35 nm-thick (1 BL) GeTe thin film grown on Si(111)-$\sqrt{3}\times\sqrt{3}$-Sb. Holes on Si(111) terraces (white arrows). (b) Height profile across a step edge [red dotted line in (a)]. The step height is 0.31 nm. (c) LEED at incident electron energy E= 16 eV showing the Si substrate and the GeTe layer diffraction patters. (d) Polar plot of the intensity of the LEED pattern at GeTe peak radial coordinate [dotted arrow in (c)]. The full width at half maximum of the spots is $\Delta\omega$ =6°. (e) Radial plot of the intensity of the LEED pattern [dashed dark line in (c)]. The GeTe and Si peaks are shown by arrows.

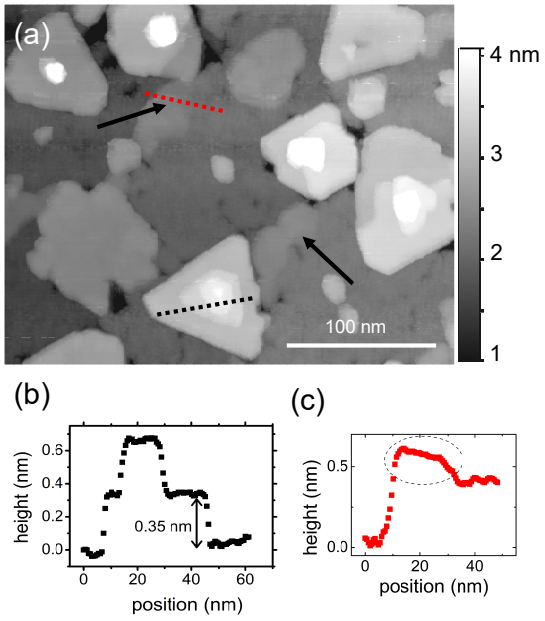

FIG. 3. (a) STM image of a GeTe thin film of 2 BL, *i.e.* when RHEED scattering rods are intense and well-defined. Black arrows: areas of smooth height variations of the surface morphology. (b) Height profile taken across step-edges (black dotted line on a GeTe island). The step height is 0.35 nm as expected for GeTe. (c) Height profile taken across the red dotted line of (a) showing a smooth height variation on the upper terrace (see red dashed oval region).

a_{Si}=0.384 nm. This value is close to the expected lattice parameter of bulk α-GeTe considering a rhombohedron axis normal to the surface. Thus the GeTe film is relaxed since the very first atomic bilayer (BL) [19]. However some disorder is observed: significant in-plane misorientations (FWHM~6°) and a diffuse scattering ring are evidenced by LEED [figure 2(c)-(d)]. In addition figure 2(a) shows a few monoatomic holes of 5-10 nm diameter on the substrate. These holes indicate that a part of the Si substrate atoms are consumed during the initial GeTe growth.

Figure 3(a) shows the STM image of a sample where the GeTe growth has been stopped when the scattering rods of the RHEED pattern of GeTe become thinner and well-defined (~ 0.7 nm, 2 BLs). We observe atomically flat islands on the surface explaining the occurrence of thin and elongated RHEED scattering rods (the buffer layer is still present in between islands). The islands nucleate preferentially at Si step edges and the step height on the islands is now 0.35 nm as expected for a GeTe BL [figure 3(b)]. The step edges of the Si substrate are strongly disturbed by the growth. It is a clear indication that the topmost Si atoms are mobile at the onset of growth. The Si mobility could result from the high tendency of alloying between Ge and Si as well as Te and Si. In addition, at some places close to step edges, the topography shows smooth height variations over ~10 nm lateral distance that are accompanied with a change of the surface aspect: flat/uphill and more grainy/downhill [see black arrows in figure 3(a) and height profile in figure 3(c)]. These local changes of the surface height could be a signature of a local activation of the Peierls distortion that was hindered for a 0.35 nm-thick film [19]. However we cannot exclude that these variations arise from composition inhomogeneities that may involve the silicon substrate and/or Sb (see supplementary materials S3 [22]).

Upon a GeTe deposition of 1 nm (~ 3 BL), STM image in figure 4(a) shows that extended and smooth islands are already formed on the whole surface. The growth is not a perfect layer-by-layer growth since new layers appear before the previous layer is complete. This observation corroborates the rapid decrease of the amplitude of the

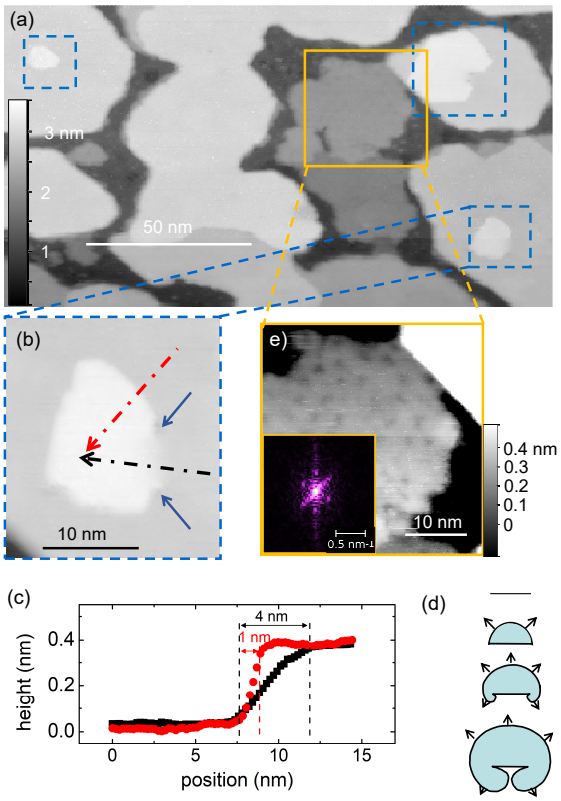

FIG. 4. (a) STM image of a 1 nm-thick (3 BL) GeTe thin film grown on Si(111)-$\sqrt{3}\times\sqrt{3}$-Sb (U= -1V; I= 20 pA). Dashed blue squares show Frank-Read source of dislocations. (b) Close view of a Frank-Read source of dislocations from (a). Blues arrows indicate the location of the two threading dislocations. (c) Height profiles along the dashed arrows in (b). The black height profile is located in between two threading dislocations with opposite Burger vectors and show a smooth height variation ($\sim$ 4 nm width). The red height profile passes across an abrupt step edge (resulting from one threading dislocation). (d) Scheme of the evolution during growth of a Frank-Read source of dislocations (surface steps). (e) Close view of a surface area showing a modulated surface topography (orange areas in (a)). Inset: Fourier transform of the morphology showing an ordered hexagonal lattice.

RHEED oscillations as shown by Wang and coworkers [19]. In addition to the layer-by-layer growth mode, we can also notice that the surface has some very distinctive surface steps consisting of curved step edges with both ends terminated by a threading dislocation (see figures 4(a)-(b)). To reach the top of the corresponding islands, two different paths can be considered: one path with an abrupt height variation (step edge) and another path with a smooth height increase over 4 nm [figure 4(c)]. The net displacement of both paths normal to the surface is 0.35 nm, *i.e.* equal to the height of a bilayer. This indicates that the threading dislocations are screw-like. In NaCl compounds, such as GeTe (considering a pseudo-cubic lattice) and for a (111) crystallographic plane, the Burgers vector of dislocations is usually $\frac{1}{2}[110]$, corresponding to the measured height displacement [23]. In this case two screw dislocations with opposite Burger vectors are formed that cancel the total normal displacement on the surface [figures 4(b)-(c)]. These structures can be referred as Frank-Read [24] sources of dislocations and generate surface steps [figure 4(d)]. We can also distinguish Moiré-like patterns on terraces [figure 4(e)]. The Fourier transform of the STM image shows a hexagonal like pattern with a lattice period of p=0.26$\pm$0.05 nm^{-1}. This pattern can be associated with a hexagonal superlattice of period $a = \frac{1}{p} \times \frac{2}{\sqrt{3}} = 4.4 \pm 1.0$ nm. Since the in-plane lattice parameter mismatch between bulk GeTe and Si is $\frac{\Delta a}{a_{Si}}$=8.3$\pm$2.5%, then the expected coincidence lattice of the relaxed layer of GeTe(111) on Si(111)-Sb with GeTe[1$\bar{1}$0] $\|$Si[1$\bar{1}$0] has a period of 4.64 nm [15]. This value matches the periodicity of the Moiré pattern. This coincidence lattice is also in adequation with the misfit dislocation network that as been characterized by HR-TEM at the GeTe/Si interface of thicker films by Croes and coworkers [18].

Already for the deposition of a 2 nm-thick GeTe film (6 BL), extended atomically flat terraces (> 50 nm) are present on the whole surface [figure 5-(a)]. As the RHEED intensity of the specular beam reaches a steady state behaviour [19] we can consider that the growth proceeds *via* a step flow mode. Adjacent terraces may be separated by slight depressions arising from the grain boundaries due to the local lattice mismatch. The step edge profiles show a 0.35 nm height as expected for a GeTe bilayer [see inset of figure 5-(a)]. Some few remaining surface steps are still arising *via* Frank-Read sources of dislocations [see dashed squares in figure 5-(a)]. As underlined in a similar system, PbTe(111) grown on BaF_2 [25], their disappearance could result from the annihilation of the dislocations pair due to their strong attractive interaction and assuming an increase of the dislocation mobility with the film thickness. We can also notice that the island step edges are smooth. For a GeTe film several tens of nanometers thick, two types of step edges exist: the straight step edge called A-step and the notched one called B-step [figure 5-(b)]. As underlined by Croes et al. [26] the occurrence of notches at the B-step edges neutralizes the electric charges. The absence of triangular notches for nanometer-thick GeTe thin films could result from the intermixing with the Sb layer deposited prior GeTe deposition that may stabilize the step edge structure. The overall growth of GeTe on Si(111) as a two dimensional film suggests that the surface energy of GeTe(111) is smaller than the difference between the surface energy of Si(111) and GeTe/Si interfacial energy. As calculated by Deringer and coworkers [27] the surface energy of the Te-terminated surface of GeTe(111) is 2.1 eV/nm^2 and the Si(111) surface energy is 9.2 eV/nm^2 [28]. The latter energy is reduced by 1.8 eV/nm^2 considering the Sb adsorption at the surface [29]. Since GeTe wets perfectly the Si substrate, these energies allow estimating a maximum value for the interfacial energy of GeTe/Si 9.2-1.8-2.1=5.3 eV/nm^2.

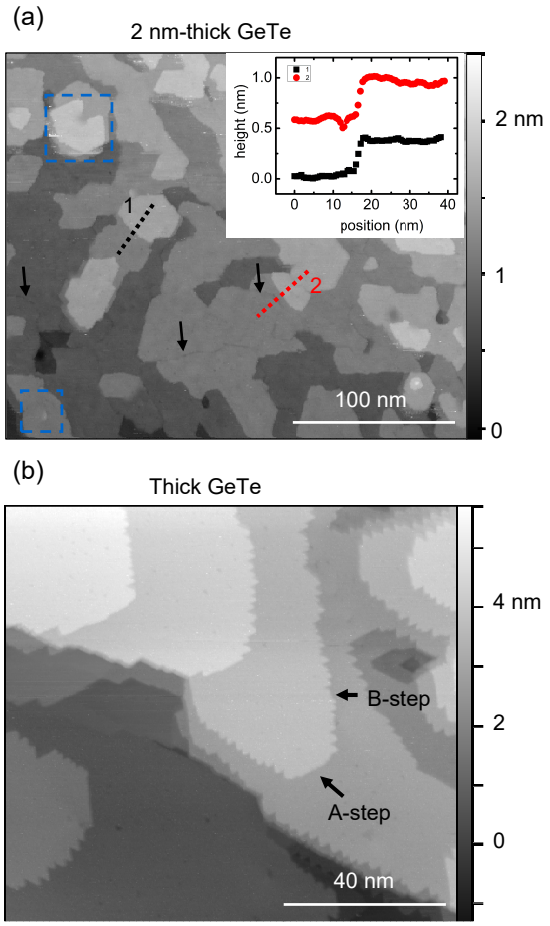

FIG. 5. (a) Large scale STM image of a 2 nm-thick GeTe thin film grown on Si(111)-$\sqrt{3}\times\sqrt{3}$-Sb (U= -1V; I= 20 pA). Slight depressions at grain boundaries (black arrows). Remaining Frank-Read sources of dislocations (dashed blue squares). Inset: bilayer step-edges. (b) STM image of a 40 nm-thick GeTe film showing notched step-edges (B-step) and smooth step-edges (A-step).

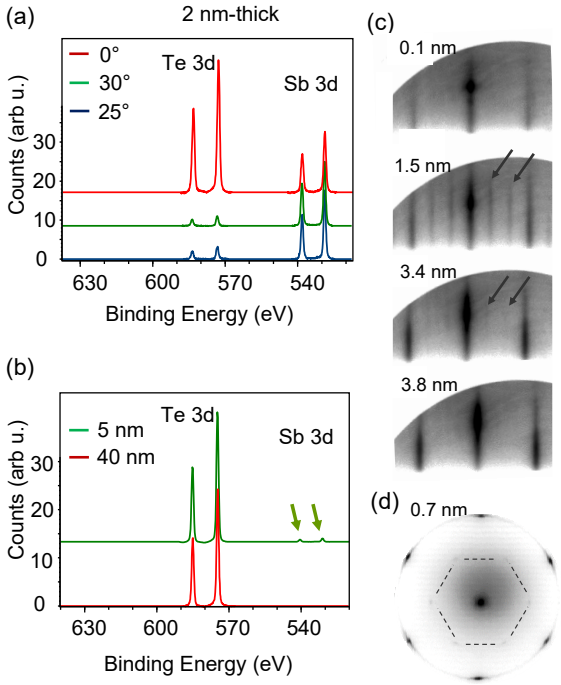

FIG. 6. (a) XPS spectra of a 2 nm-thick GeTe film at different exit angles of photo-emitted electrons. (b) XPS spectra of a 5 nm- and a 40 nm-thick GeTe films at 0° exit angle. The arrows show the Sb $3d_{3/2}$ and Sb $3d_{5/2}$ peaks of the 5 nm-thick sample. (c) RHEED patterns at the beginning of the growth of GeTe : from 0.1 nm to 3.8 nm deposited film. Arrows point to additional rods that appear a few tens of seconds after the beginning of the growth and disappear a few minutes later. (d) LEED pattern for a 0.7 nm-thick GeTe thin film. Si(111)-$\sqrt{3}\times\sqrt{3}$-Sb reconstruction (dashed hexagon).

B. Sb surfactant role, mosaicity and mirror domains

To address the chemical composition of the film during the initial stages of GeTe growth, we have made XPS measurements at Sb 3d and Te 3d binding energies considering an incident photon energy of 800 eV. Sb contributions ($3d_{3/2}$ and $3d_{5/2}$) can be seen on the XPS spectrum for a 2-nm thick GeTe film [figure 6-(a)]. By increasing the XPS sensitivity to the sample surface, increasing the exit angle of detection of the photo-emitted electrons with respect to the surface normal, we see that the Te 3d peaks nearly vanish while the intensity of Sb peaks increases. This result shows that a significant amount of Sb is located in the surface region. To rule out possible photodiffraction effects we have made measurements at two incident angles (25° and 30°). For a 5 nm-thick film, the Sb peak still shows a faint contribution and it is completely absent for a 40 nm-thick film [figures 6-(b)]. Therefore Sb is progressively buried inside the GeTe film during growth. In addition to spectroscopy the presence of Sb at the surface is correlated with the occurrence of additional peaks on the RHEED and LEED patterns [figures 6-(c)-(d)]. Those peaks can be attributed to a $\sqrt{3}\times\sqrt{3}$ reconstruction of the GeTe surface [15]. The reconstruction is visible up to a ∼4 nm-thick GeTe layer that is close to the detection limit of Sb by XPS indicating that the reconstruction is promoted by the presence of Sb at the surface. In addition this reconstruction is not detected when GeTe is grown on Si(111) without the deposition of 1 monolayer of Sb [30]. Therefore the presence of Sb favors the layer-by-layer and step flow growth modes by acting as a surfactant during the early stages of growth. This result is corroborated by previous studies on the surfactant effect of Sb, *e.g.* during growth of Ge layers on Si(111) [31 and 32]. The favorable termination of the growing layer with Sb at the growth front prevents the formation of islands to relax the elastic stress due to the lattice mimatch. In such surfactant-mediated epitaxy a complete relaxation of the interface *via* misfit dislocations is favored [33 and 34].

We can infer that a similar mechanism is occurring in the case of GeTe growth on Si(111)-Sb.

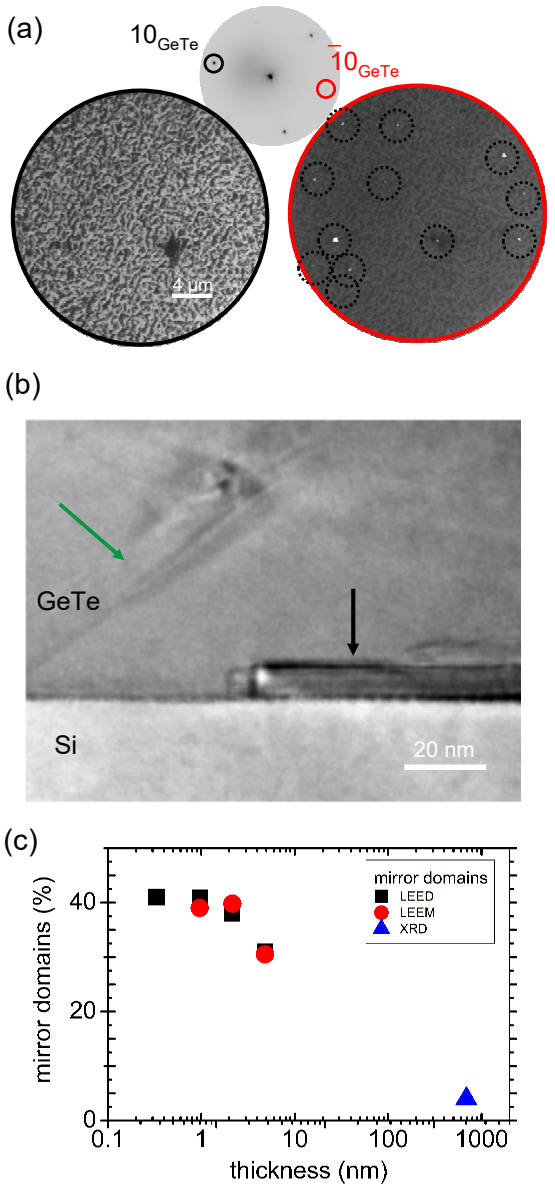

FIG. 7. (a) Dark-field LEEM images of a 460 nm-thick GeTe film measured with 26 eV electron incident energy and using 10 (left image) and $\bar{1}0$ (right image) GeTe spots. The LEED pattern is in the middle (above). Due to the threefold symmetry of the GeTe crystalline structure, a strong intensity difference between 10 and $\bar{1}0$ occurs. The intensity difference is maximum for 26 eV energy incident electrons. The mirror domains are detected using the $\bar{1}0$ LEED spot for imaging using 26 eV electrons (dark dashed circles in right image). (b) TEM cross-section of a 200 nm-thick GeTe film. The black arrow points to a mirror domain buried at the interface with silicon. The green arrow shows a ferroelectric nanodomain crossing the GeTe film (see also [18]). (c) Evolution of the fraction of mirror domains with film thickness as measured by LEED and LEEM (below 5 nm) and X-ray diffraction (> 40 nm).

To evaluate the crystalline quality of nanometer-thick GeTe film we have characterized the evolution of the fraction of mirror domains (ACB stacking instead of ABC) and in-plane misorientation (mosaicity). For a 460 nm-thick GeTe film, the LEED pattern shows sharp diffraction spots demonstrating that the mosaicity is below 1° (figure 7-(a) and [26]). In addition LEEM images using dark-field imaging mode on major and minor diffraction peaks show that only a very small fraction of mirror domains can be detected. These results are confirmed by TEM [see figure 7-(b)]. For nanometer-thick GeTe thin films, the fraction of mirror domains have been measured by LEED. Indeed the LEED pattern at 26 eV shows six diffraction spots at 60° and a threefold symmetry considering the peak intensities. Therefore the mirror domain ratio can be estimated by measuring the intensity ratio between two peaks at 60° called 10 and $\bar{1}0$ using 26 eV incident electrons. We deduce that there is about 41% of mirror domains for a 0.28 nm-thick film, and this value decreases to ∼31% for a 2.8 nm-thick film [figure 7-(c)]. Considering a large range of film thickness studied by X-ray diffraction and LEED we can deduce that the mirror domain ratio drops with the film thickness [see figure 7-(c)]. Even though the initial GeTe film has a significant amount of defects, they are rapidly buried at the interface with the Si substrate [see TEM image in figure 7-(b)]. At the beginning of growth, the fraction of mirror domains is slightly below one half indicating that GeTe is able to interact with the 3-fold symmetry of the substrate [15]. However the strongest effect seems to be related to the kinetics of growth that allows the main domain to rapidly bury the mirror domains. Considering the mosaicity of the GeTe films, the 3D reciprocal space map of a 200 nm-thick GeTe film around a non-symmetric Bragg peak 202_h [see figure 8-(a)] shows a slight in-plane misorientation of 1.2° (FWHM=0.5±0.1° for a 800 nm-thick sample). We can also notice that 3 additional peaks are found nearby the main GeTe peak. They arise due to the presence of GeTe ferroelastic domains [18]. The in-plane broadening of the Bragg peaks show that the misorientations also impact the ferroelastic domains and the mirror domains [see figure 8-(b)]. For nanometer-thick GeTe thin films, the mosaicity has been measured by LEED (see supplementary materials S4 [36]). The low energy electron scattering ring measured for a 0.28 nm-thick film (0.8 bilayer) begins to disappear at the second bilayer (0.7 nm) and is not present at the fourth bilayer (1.4 nm). The polar plot of the full width at half maximum of the diffraction peaks shows that the misorientation decreases with the film thickness from 5.8° ±0.2° to 4.7° ±0.2° respectively for 0.28 and 2.8 nm-thick films [figure 8-(c)]. Considering a large range of film thickness studied by X-ray diffraction and LEED we can see that the in-plane misorientation decreases with the film thickness [see figure 8-(c)]. To suppress the mirror domains and misorientations between adjacent grains since the beginning of growth we have used Si substrates slightly miscut with respect to Si(111). The vicinal Si(556) substrate is

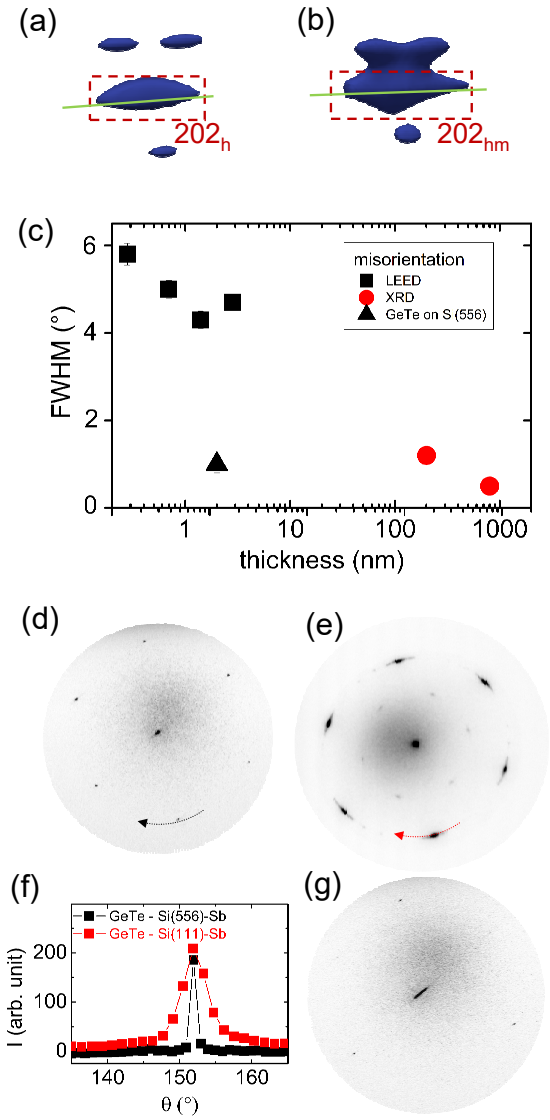

FIG. 8. (a)-(b) 3D reciprocal space maps of GeTe 202_h and GeTe 202_{hm} Bragg peaks of GeTe thin film grown on Si(111)-Sb and obtained by X-ray diffraction (200 nm-thick sample). h stands for hexagonal unit cell of the main GeTe domain and hm for the mirror domains. Around the main Bragg peaks, additional spots arise due to the presence of ferroelastic domains [18 and 35]. The Bragg peaks are elongated in-plane due to a residual in-plane mosaicity of the GeTe film. (c) Evolution of the in-plane mosaicity (full width at half maximum) with the film thickness as measured by LEED (below 5 nm) and X-ray diffraction (> 40 nm). (d) LEED pattern of a 2 nm-thick GeTe thin film grown on Si(556)-Sb. Incident electron energies: 16 eV. (e) LEED pattern of a 1.4 nm-thick GeTe thin film grown on Si(111)-$\sqrt{3}\times\sqrt{3}$-Sb. Incident electron energy: 16 eV. (f) Polar plots along the LEED diffraction peaks from GeTe grown on Si(556)-Sb [see image (d)] and Si(111)-Sb [see image (e)].(g) LEED pattern of a 2 nm-thick GeTe thin film grown on Si(556)-Sb. Incident electron energies: 26 eV. The pattern has a clear 3-fold symmetry.

tilted by 5° with respect to the (111) plane in the $[\overline{1}\overline{1}2]$ direction. Figures 8-(d)-(e) show a comparison between the LEED patterns with 16 eV incident electrons of GeTe ultrathin films grown on Si(556)-Sb and on Si(111)-Sb. Very sharp diffraction spots are measured on the miscut substrate and the $\sqrt{3}\times\sqrt{3}$-Sb is absent. This result indicates that the misorientations are strongly suppressed [below 1°, see figure 8-(f)]. In addition the LEED pattern, using 26 eV incident electrons, of the GeTe ultrathin film grown on the miscut substrate shows a very strong asymmetry of intensity between two adjacent peaks at 60° [figure 8-(g)]. This result clearly indicates that mirror domains are also suppressed. We can thus assess that

[1] D. Di Sante, P. Barone, R. Bertacco, and S. Picozzi, Electric Control of the Giant Rashba Effect in Bulk GeTe, Adv. Mater., 25, 509 (2013).

[2] M. Liebmann, C. Rinaldi, D. Di Sante, J. Kellner, C. Pauly, R. N. Wang, J. E. Boschker, A. Giussani, S. Bertoli, M. Cantoni, L. Baldrati, M. Asa, I. Vobornik, G. Panaccione, D. Marchenko, J. Sánchez-Bariga, O. Rader, R. Calarco, S. Picozzi, R. Bertacco, and M. Morgenstern, Giant Rashba-Type Spin Splitting in Ferroelectric GeTe(111) Adv. Mater., 28, 560 (2016).

[3] J. Krempaský, S. Muff, F. Bisti, M. Fanciulli, H. Volfová, A. P. Weber, N. Pilet, P. Warnicke, H. Ebert, J. Braun, F. Bertran, V. V. Volobuev, J. Minár, G. Springholz, J. H. Dil, and V. N. Strocov, Entanglement and manipulation of the magnetic and spin-orbit order in multiferroic Rashba semiconductors Nat. Commun., 7, 13071 (2016).

[4] J. Krempaský, H. Volfová, S. Muff, N. Pilet, G. Landolt, M. Radovic, M. Shi, D. Kriegner, V. Holý, J. Braun, H. Ebert, F. Bisti, V. A. Rogalev, V. N. Strocov, G. Springholz, J. Minár, and J. H. Dil, Disentangling bulk and surface Rashba effects in ferroelectric alpha-GeTe, Phys. Rev. B, 94, 205111 (2016).

[5] G. Kremer, T. Jaouen, B. Salzmann, L. Nicolaï, M. Rumo, C. W. Nicholson, B. Hildebrand, J. H. Dil, J. Minár, G. Springholz, J. Krempaský, C. Monney, Unveiling the complete dispersion of the giant Rashba split surface states of ferroelectric α-GeTe(111) by alkali doping, Phys. Rev. Research 2, 033115 (2020).

[6] A. V. Kolobov, D. J. Kim, A. Giussani, P. Fons, J. Tominaga, R. Calarco, and A. Gruverman, Ferroelectric switching in epitaxial GeTe films, APL Mater., 2, 066101 (2014).

[7] C. Rinaldi, S. Varotto, M. Asa, J. Slawinska, J. Fujii, G. Vinai, S. Cecchi, D. Di Sante, R. Calarco, I. Vobornik, G. Panaccione, S. Picozzi, and R. Bertacco, Ferroelectric Control of the Spin Texture in GeTe, Nano Lett. 18, 2751 (2018).

[8] J. Krempasky, S. Muff, J. Minar, N. Pilet, M. Fanciulli, A. P. Weber, E. B. Guedes, M. Caputo, E. Mueller, V. V. Volobuev, M. Gmitra, C. A. F. Vaz, V Scagnoli, G. Springholz, and J. H. Dil, Operando Imaging of All-Electric Spin Texture Manipulation in Ferroelectric and Multiferroic Rashba Semiconductors, Phys. Rev. X 8, 021067 (2018).

[9] Y. Li, Y. Li, P. Li, B. Fang, X. Yang, Y. Wen, D.-X. Zheng, C.-H. Zhang, X. He, A. Manchon, Z.-H. Cheng, and X.-X. Zhang, Nonreciprocal charge transport up to room temperature in bulk Rashba semiconductor alpha-GeTe, Nat. Commun. 12, 540 (2021).

[10] Sara Varotto, Luca Nessi, Stefano Cecchi, Jagoda Slawinska, Paul Noel, Simone Petro, Federico Fagiani, Alessandro Novati, Matteo Cantoni, Daniela Petti, Edoardo Albisetti, Marcio Costa, Raffaella Calarco, Marco Buongiorno Nardelli, Manuel Bibes, Silvia Picozzi, Jean-Philippe Attane, Laurent Vila, Riccardo Bertacco, and Christian Rinaldi, Room-temperature ferroelectric switching of spin-to-charge conversion in germanium telluride, Nature electronics 4, 740 (2021).

[11] A. V. Kolobov, P. Fons, M. Krbal, J. Tominaga, A. Giussani, K. Perumal, H. Riechert, R. Calarco, T. Uruga, Local structure of epitaxial GeTe and Ge2Sb2Te5 films grown on InAs and Si substrates with (100) and (111) orientations: An x-ray absorption near-edge structure study, J. Appl. Phys. 117, 125308 (2015)

[12] Karthick Perumal, Epitaxial growth of Ge-Sb-Te based phase change materials, PhD thesis, Humboldt-Universität zu Berlin, Mathematisch-Naturwissenschaftliche Fakultät I (2013).

[13] Alessandro Giussani, Karthick Perumal, Michael Hanke, Peter Rodenbach, Henning Riechert, Raffaella Calarco, On the epitaxy of germanium telluride thin films on silicon substrates, Physica Status Solidi B 249, 1939 (2012).

[14] Jamo Momand, Jos E. Boschker, Ruining Wang, Raffaella Calarco, Bart J. Kooi, Tailoring the epitaxy of Sb2Te3 and GeTe thin films using surface passivation, CrystEngComm 20,340 (2018).

[15] R. Wang, J. E. Boschker, E. Bruyer, D. Di Sante, S. Picozzi, K. Perumal, A. Giussani, H. Riechert, and R. Calarco, Toward Truly Single Crystalline GeTe Films: The Relevance of the Substrate Surface, J. Phys. Chem. C 118, 29724 (2014).

[16] R. T. Lechner, G. Springholz, M. Hassan, H. Groiss, R. Kirchschlager, J. Stangl, N. Hrauda, G. Bauer, Phase separation and exchange biasing in the ferromagnetic IV−VI semiconductor $Ge_{1-x}Mn_xTe$, Applied Physics Letters 97, 023101 (2010).

[17] M. Hassan, G. Springholz , R. T. Lechner , H. Groiss, R. Kirchschlager, G. Bauer, Molecular beam epitaxy of single phase GeMnTe with high ferromagnetic transition temperature, J. Cryst. Growth 323, 363 (2011).

[18] B. Croes, F. Cheynis, Y. Zhang, C. Voulot, K. D. Dorkenoo, S. Cherifi-Hertel, C. Mocuta, M. Texier, T. Cornelius, O. Thomas, M.-I. Richard, P. Müller, S. Curiotto, and F. Leroy, Ferroelectric nanodomains in epitaxial GeTe thin films, Phys. Rev. Materials 5, 124415 (2021).

[19] Ruining Wang, Davide Campi, Marco Bernasconi, Jamo Momand, Bart J. Kooi, Marcel A. Verheijen, Matthias Wuttig, and Raffaella Calarco, Ordered peierls distortion prevented at growth onset of GeTe ultra-thin films, Sci. Rep. 6, 32895 (2016).

[20] See Supplemental Material S1 at [publisher address] for LEED measurements before and after Te desorption.

[21] See Supplemental Material S2 at [publisher address] for electric conductivity measurements of GeTe thin film as function of temperature.

[22] See Supplemental Material S3 at [publisher address] for XPS dataset around Si core level binding energies.

[23] John Price Hirth and Jens Lothe, Theory of Dislocations, Krieger Publishing Company (1992).

[24] F. C. Frank and W. T. Read, Multiplication Processes for Slow Moving Dislocations, Phys. Rev. 79, 722 (1950).

[25] G Springholz, AY Ueta, N Frank, and G Bauer, Spiral growth and threading dislocations for molecular beam epitaxy of PbTe on BaF_2(111) studied by scanning tunneling microscopy, Appl. Phys. Lett. 69, 2822 (1996).

[26] B. Croes, F. Cheynis, P. Müller, S. Curiotto, and F. Leroy, Polar surface of ferroelectric nanodomains in GeTe thin films, Phys. Rev. Materials 6, 064407 (2022).

[27] V. L. Deringer, M. Lumeij, and R. Dronskowski, Ab Initio Modeling of alpha-GeTe(111) Surfaces, J. Phys. Chem. C 116, 15801 (2012).

[28] R. Zhachuk, J. Coutinho, A. Dolbak, V. Cherepanov, and B. Voigtländer, Si(111) strained layers on Ge(111): Evi-

dence for c(2× 4) domains, Phys. Rev. B 96, 085401 (2017).
[29] H. Guesmi, L. Lapena, G. Tréglia, and P. Müller, Coverage dependence of Sb/Si(111) adsorption and desorption modes: Interplay between chemical interactions and site transitions, Phys. Rev. B 77, 085402 (2008).
[30] Alessandro Giussani, Karthick Perumal, Michael Hanke, Peter Rodenbach, Henning Riechert, and Raffaella Calarco, On the epitaxy of germanium telluride thin films on silicon substrates, Phys. Status Solidi B 249, 1939 (2012).
[31] M. Hornvonhoegen, F. K. Legoues, M. Copel, M. C. Reuter, R. M. Tromp, Defect self-annihilation in surfactant-mediated epitaxial growth, Phys. Rev. Lett. 67, 1130 (1991).
[32] B. Voigtländer, and A. Zinner, Surfactant mediated epitaxy of Ge on Si(111): The role of kinetics and characterization of the Ge layers, Journal of Vacuum Science & Technology A 12, 1932 (1994).
[33] G. Meyer, B. Voigtländer, and N.M. Amer, Scanning tunneling microscopy of surfactant-mediated epitaxy of Ge on Si(lll): strain relief mechanisms and growth kinetics, Surface Science 274, L541 (1992).
[34] G. Meyer, B. Voigtländer, and N.M. Amer, Strain-relief mechanism in surfactant-grown epitaxial germanium films on Si(111), Phys. Rev. B 44, 12894 (1991).
[35] D. Kriegner, G. Springholz, C. Richter, N. Filet, E. Mueller, M. Capron, H. Berger, V. Holy, J. H. Dil, and J. Krempasky, Ferroelectric Self-Poling in GeTe Films and Crystals, Crystals 9, 335 (2019).
[36] See Supplemental Material S4 at [publisher address] for LEED patterns and polar plots as function of film thickness.
[37] Eugenio Zallo, Stefano Cecchi, Jos E. Boschker, Antonio M. Mio, Fabrizio Arciprete, Stefania Privitera, and Raffaella Calarco, Modulation of van der Waals and classical epitaxy induced by strain at the Si step edges in GeSbTe alloys, Sci. Rep. 7, 1466 (2017).
[38] Fabrizio Arciprete, Jos Emiel Boschker, Stefano Cecchi, Eugenio Zallo, Valeria Bragaglia, and Raffaella Calarco, Hints for a General Understanding of the Epitaxial Rules for van der Waals Epitaxy from Ge-Sb-Te Alloys, Adv. Mater. Interfaces 9, 2101556 (2022).